Available online at www.sciencedirect.com

SciVerse ScienceDirect

Journal of the European Ceramic Society 32 (2012) 2399–2404

www.elsevier.com/locate/jeurceramsoc

The formation of secondary phases in $Bi_{0.5}Na_{0.375}K_{0.125}TiO_3$ ceramics

Michael Naderer [a], Denis Schütz [a], Theresa Kainz [a], Klaus Reichmann [a,*], Florian Mittermayr [b]

[a] *Graz University of Technology, Christian Doppler Laboratory for Advanced Ferroic Oxides, Stremayrgasse 9, 8010 Graz, Austria*
[b] *Graz University of Technology, Institute of Applied Geosciences, Rechbauerstraße 12, 8010 Graz, Austria*

Received 2 September 2011; received in revised form 17 February 2012; accepted 20 February 2012
Available online 17 March 2012

Abstract

The synthesis of $Bi_{0.5}Na_{0.375}K_{0.125}TiO_3$ (BNT–BKT or NBT-KBT) by the mixed oxide route was investigated using thermogravimetry, X-ray diffraction, scanning electron microscopy and electron microprobe analysis. The results show the formation of a paraelectric secondary phase with the composition $(K,Na)_2Ti_6O_{13}$ during sintering. Thermogravimetric measurements indicate that the main loss of volatile components mainly occurs during the calcinations step, exceeding the theoretical loss by more than 2%. These losses, most likely caused by evaporation of K_2O induce a high number of Schottky-vacancies. These vacancies highly affect the electrical properties of the material. The formation of the secondary phase leads to a shifted composition of the ceramic to approximately $Bi_{0.5}Na_{0.4}K_{0.1}TiO_3$.

Keywords: BNT; Lead-free; Inclusions; Electron microscopy; Dielectric properties

1. Introduction

$Bi_{0.5}Na_{(0.5-x)}K_xTiO_3$ (short BNT–*x*BKT) is a promising candidate to replace lead-based materials in ferroelectric applications.[1–3] According to the RoHS-guideline, the use of materials with serious health risks is prohibited as soon as alternative materials are technically available. Structurally, BNT–*x*BKT forms a complex perovskite with a mixed A-site occupation (bismuth, potassium and sodium) and titanium as single ion on the B-site. BNT and BKT form solid solutions of various crystal symmetries in dependence of the ratio BNT:BKT. High amounts of BNT form a rhombohedral phase, while BKT-rich compositions are tetragonal. Pure BNT is also reported to be monoclinic.[4] The morphotropic phase boundary (MPB), where piezoelectric parameters are maximized is located between ratios of 16 and 20% BKT.[5–7]

Bismuth-alkali titanates (e.g. bismuth–sodium–titanate BNT or bismuth–potassium–titanate BKT) are known to form secondary phases during thermal processing. In literature different compositions for this phase are given, but the general trend is to higher amounts of Ti compared to BNT–*x*BKT. The difference in composition of the secondary phase can be explained with the diverse fabrication techniques of the ceramic, especially the highest temperature during calcination and sintering and of course the method of measurement. Proposed compositions are $K_2Ti_8O_{17}$ in BNT–BKT,[8] $NaBiTi_6O_{14}$ in BNT,[9] $K_2Ti_6O_{13}$ in BKT[10] or $K_2Na_4(TiO_3)_3$ in BNT–BT–KNN (BT: barium–titanate, KNN: potassium–sodium–niobate).[11]

The composition of the secondary phase found in this work can be written as $(Na, K)_2Ti_6O_{13} + xBi_2O_3$ with a strongly temperature dependent stoichiometric factor *x* for Bi_2O_3. Samples sintered at temperatures below 1050 °C show relatively high amounts of Bi_2O_3 in the secondary phase, at higher temperatures only traces of Bi_2O_3 can be found. A mechanism for this behavior will be presented. The secondary phase itself seems to have no influence on the electrical properties, the formation reaction and the resulting compositional shift therefore have an high impact for compositions close to the MPB.

2. Experimental

The compound was synthesized using a conventional mixed-oxide route. Stoichiometric quantities of reagent grade K_2CO_3 (99.99, Ferro GmbH), Na_2CO_3 (99.99, Merck), Bi_2O_3 (99.9, MCP-HEK GmbH) and TiO_2 (99.8%, Tronox) were mixed together and ball-milled in a planetary mill (Fritsch PULVERISETTE4). Since the alkali carbonates are soluble in water,

* Corresponding author. Tel.: +43 316 873 32321; fax: +43 316 873 1032321.
E-mail address: k.reichmann@tugraz.at (K. Reichmann).

0955-2219/$ – see front matter © 2012 Elsevier Ltd. All rights reserved.
doi:10.1016/j.jeurceramsoc.2012.02.031

ethanol was used for this step. The ball milling was carried out in 5 cycles of 10 min milling and 10 min break to let the suspension cool down and prevent the evaporation of ethanol. In this milling step, yttrium-stabilized ZrO_2 balls with 5 mm diameter were used. Since K_2CO_3 and Na_2CO_3 are hygroscopic, these materials were dried at 250 °C and cooled in a desiccator over silica gel before weighing. After milling ethanol was removed from the suspension using a rotary evaporator and a drying oven at 120 °C.

The dry mixture was grinded and sieved to an agglomerate size less than 180 μm and put in an alumina crucible. The calcination step took place in a box furnace (Carbolite CWF 1300) with a first stage of 650 °C and a final stage of 950 °C to ensure the completion of the reaction. Heating rates for the calcination were 5 K/min, dwell time at both temperatures 120 min. The completion of this reaction was checked by X-ray diffraction (XRD) (Bruker AXS D5005 y-y, Cu Kα emitter, graphite secondary monochromator). Further analysis of the calcination reaction was done with a thermogravimetrical analysis coupled with differential scanning calorimetry (TGA-DSC) (Netzsch STA 409 CD with Aeolus masspectrometer) to measure the weight loss, the emanating gases and to determine the temperature levels for the reaction.

Subsequently, the material was ball-milled in ethanol using the planetary mill to reduce particle size. To ease this process, a dispersant (Dispex A40, Ciba Spezialitaetenchemie) was added. To ensure a small particle size, applied energy was higher compared to the first milling due the use of 2 mm yttrium-stabilized ZrO_2 balls and higher rotational speeds. The drying step was equivalent to the one after the first milling step. The agglomerate size was then reduced to 180 μm using test sieves. Before pressing the powder into discs with a diameter of 13 mm, 5 wt% of a binding aid (PEG20000, Alfa Aesar) were added.

The discs were pressed with 150 MPa for 5 min. To remove the binder before sintering, the samples were heated up to 450 °C in an open crucible, causing the thermal decomposition of the binding agent to CO_2 and H_2O. After that, the crucible was covered to reduce material losses due to evaporation of volatile components during sintering. Experiments with discs lying in powder of the same composition during sintering were also carried out; the effect on growth of the secondary phases was negligible.

Sintering temperatures were varied between 1000 °C and 1150 °C for duration of 5 h in oxidising atmosphere. After sintering, the density of the discs was measured. Preferred is Archimedes' method (Mettler Toledo XS204 DeltaRange), because geometric dimensions have no influence here. However, for samples below 1100 °C sintering temperature this method was not applicable because of the poor density. In this case, the geometric density was calculated using the thickness, diameter measured with a calliper rule (Mitutoyo CD-15DCX) and weight of the discs (Acculab ALC210.4). Due to shape irregularities of the samples, this method cannot deliver results as exact as the Archimedes' method.

For further XRD analysis, the sintered samples were ground in an agate mortar to a fine powder. For scanning electron microscopy (SEM) investigations (Zeiss Ultra 55), the discs were cut, grinded and polished with silica gel and coated with a carbon layer. This preparation was also used for the analysis with the electron microprobe (EMPA) with wavelength dispersive X-ray spectroscopy (JEOL JXA 8200).

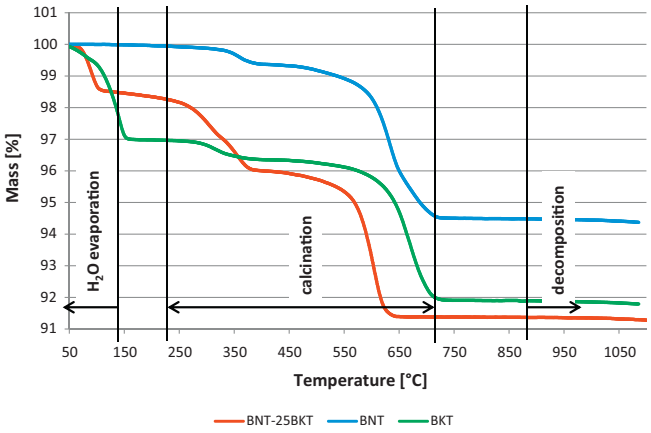

Fig. 1. TGA of BKT, BNT and BNT–25BKT raw materials mixtures. All compositions were milled in ethanol prior to measuring. Potassium containing mixtures take up water during processing.

For permittivity measurement (HP 4192A LF Analyzer) the samples were coated with silver-paste and measured at 1 kHz with 1 V. Polarization and strain measurements were performed on an aixACCT aixPES system. Samples were lapped and sputtered with a gold layer. The electric field was applied with a frequency of 0.1 Hz (triangle shape).

3. Results and discussion

Fig. 1 shows the progress of the weight loss measured with TGA. The emanation of H_2O and CO_2 was monitored with MS. Below 150 °C water evaporates, the following weight losses between 250 °C and 750 °C were assigned to the elimination of CO_2. At temperatures >1050 °C, the ceramic starts to decompose, the losses here are assumed to be mostly caused by evaporation of Bi_2O_3 and, to a smaller fraction, M_2O (M = Na, K).

The calculated weight losses caused by CO_2 are shown in Table 1; the measured values are considerably higher for BNT–25BKT. Pure BNT and BKT show almost no excess losses. The measured losses correspond to the difference between the mass after the heat treatment and the mass after the evaporation of water.

Fig. 1 also shows that the powder mixture takes up a lot of water during processing when containing potassium (see weight loss below 150 °C). The used K_2CO_3 is very hygroscopic and therefore takes up humidity of the air, as well as water from the

Table 1
Weight losses of raw materials mixtures during TGA experiment.

	Calculated [%]	Measured [%]	Difference [%]
BKT	4.76	5.04	0.28
BNT	4.94	5.23	0.29
BNT–25BKT	4.89	7.15	2.26

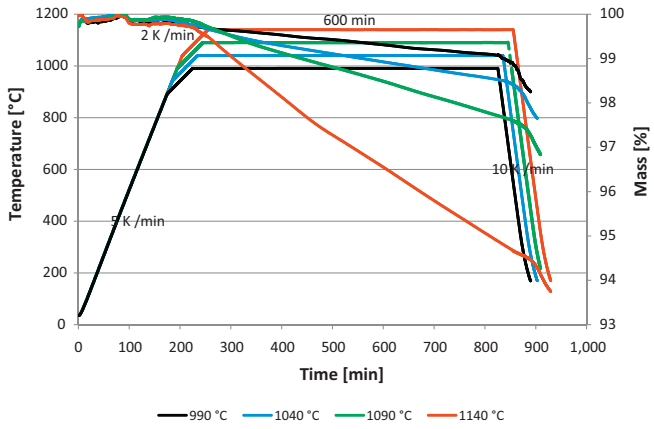

Fig. 2. TGA diagrams at constant temperature for 10 h duration at different temperatures. The used samples were made of calcined powder, pressed to pellets with 150 MPa without binding agent. The dashed lines show the used temperature profile, and the solid lines show the weight loss of the sample.

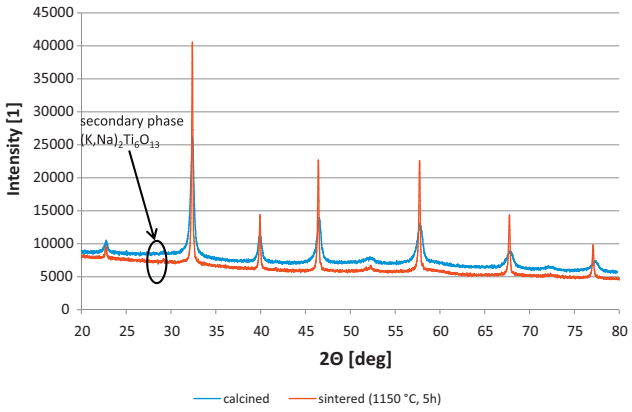

Fig. 3. XRD pattern of calcined (upper spectrum) and sintered (lower spectrum) sample. The secondary phase is visible at 29°; the sintered sample shows improved crystallinity than calcined powder.

used ethanol. Since Na_2CO_3 is not as hygroscopic as K_2CO_3, this effect is far less pronounced in pure BNT.

The complete calcination reaction, carried out in 2 steps at 650 °C and 900 °C can be formulated with Eq. (1):

$$0.25Bi_2O_3 + 0.1875Na_2CO_3 + 0.0675K_2CO_3 + TiO_2 \rightarrow Bi_{0.5}Na_{0.375}K_{0.125}TiO_3 + 0.25CO_2 \quad (1)$$

The additional weight loss in BNT–25BKT during calcination, assumed to be caused by evaporation of K_2O, which decomposes at 350 °C[12] would lead to the formation of a high concentration of vacancies in the material as described in Eq. (2).

$$0.25Bi_2O_3 + 0.1875Na_2CO_3 + 0.0675K_2CO_3 + TiO_2 \rightarrow Bi_{0.5}Na_{0.375}K_{0.125-x}V'_{(K)x}TiO_{3-(x/2)}V_{O(x/2)}^{\bullet\bullet} + \frac{x}{2}K_2O + 0.25CO_2 \quad (2)$$

This high amount of vacancies, both on the monovalent A-site and the oxygen site of the perovskite is prone to destabilize the lattice. Further the evaporation of K_2O causes a shift in A/B-ratio. Eq. (3) shows the formation of a secondary phase of alkali-polytitanate from the starting compounds, which would reduce the number of vacancies in the perovskite phase and reduces the deviation of the A/B-ratio. The formation of the secondary phase also starts at temperatures below 1000 °C. M refers to Na^+ and K^+ since these elements are chemically very much alike.

$$M_2O + 6TiO_2 \rightarrow M_2TiO_6O_{13} \quad (3)$$

Under sintering conditions, the material starts to decompose and again shows weight loss. This reaction already starts at a temperature of 990 °C as seen in Fig. 2 and is caused by the vacancies introduced during calcination. Sintering in air reduces the amount of oxygen vacancies and leads to decomposition of the material in order to keep charge neutrality. This reaction can be observed with TGA because of the occurring loss of bismuth and alkali metals.[11] The decomposition is obviously a continuous process, since the weight loss is linear over duration of 10 h.

The XRD patterns (Fig. 3) of both the calcined powder and a sample sintered at 1150 °C for a duration of 5 h show small peaks at 29°, caused by the secondary phase. Due to the loss of K_2O during the calcination, the matrix is now close to the morphotropic phase boundary and the symmetry of the matrix cannot be described as purely tetragonal or rhomboedric.

The secondary phase was investigated using SEM and electron microprobe analysis. Because it contains low amounts of bismuth compared to the matrix, it is clearly visible as dark inclusions when imaging backscattered electrons with SEM. This difference is also shown in the mapping image received from the electron microprobe analysis.

Fig. 4 shows SEM images of samples sintered at temperatures between 1000 °C and 1150 °C for 5 h. All samples show secondary phase inclusions, the lower density at low sintering temperatures is also clearly visible. In the following mappings the distribution of the metal ions around such an inclusion of a secondary phase is shown. We also found traces of zirconium in the sample, which contaminates the material during the second milling. The amount of zirconium in the matrix is low with 0.65 mol% compared to the secondary phase, where it reaches 1.96 mol%. The matrix material and the secondary phases appear to be very homogenous. The apparent diffusion zone is an artifact introduced through the interaction volume of the electron beam during excitation of the material, as with any beam based method.[13]

The mapping in Fig. 5 clearly shows the different compositions of matrix an secondary phase. As reference materials the mineral sanidine, Bi_2O_3, TiO_2 and ZrO_2 were used. All elements were quantified using WDS, acceleration voltage was set to 15 kV at a working distance of 11.0250 mm. The elemental composition of the ceramic and the secondary phase is summarized in Table 2.

Table 2 shows, that at 1100 °C sintering temperature, the composition is no longer BNT–25BKT (0.75BNT–0.25BKT) but 0.78BNT–0.22BKT. At 1150 °C the shift is even larger to BNT–17BKT (0.83BNT–0.17BKT). This shift is caused by the loss of K_2O during the calcination and the decomposition according to Eq. (4) during sintering. The loss of monovalent

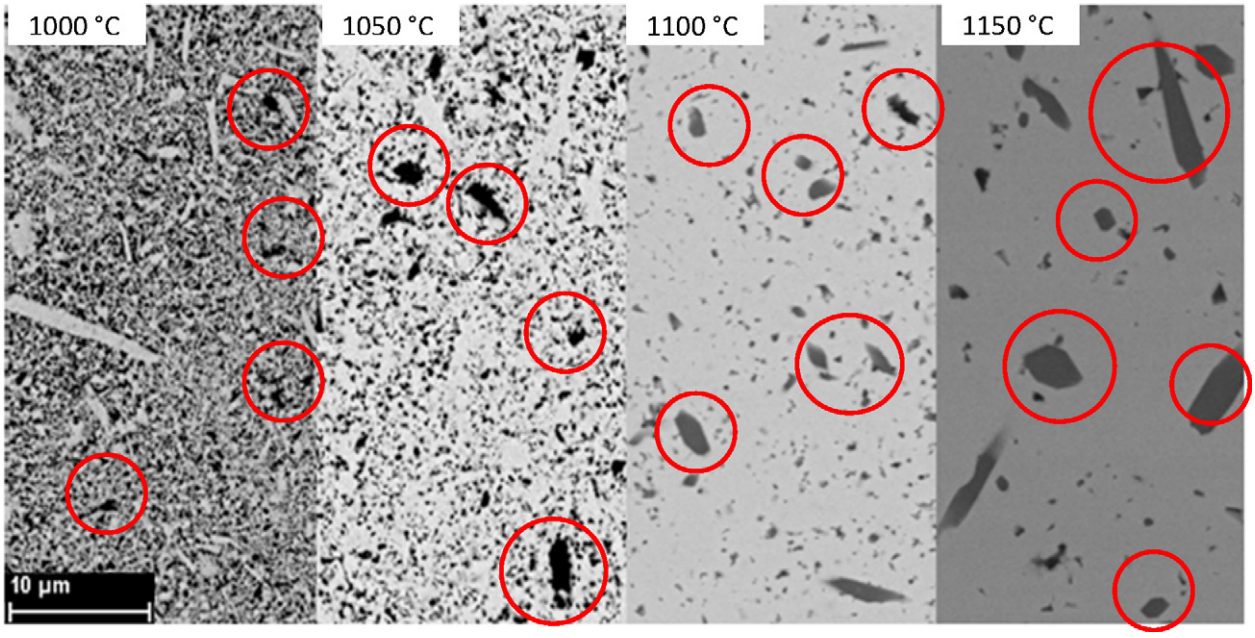

Fig. 4. SEM image of matrix and secondary phase (red circles, dark inclusions). The density visibly rises at higher sintering temperatures. (For interpretation of the references to color in this figure legend, the reader is referred to the web version of this article.)

A-site ions leads to instability of the system at higher temperatures.

The secondary phase consists of a polytitanate with a constant ratio of alkali ion:titanium of 1:3. At sintering temperatures below 1100 °C, Bi is also present in this phase. The data also confirm that the formation of the secondary phase occurs during calcination and again above 1050 °C as a result of the decomposition of the material. The higher the sintering temperature, the lower the Bi-content of the secondary phase, which indicates that the source of the weight loss at temperatures >1050 °C

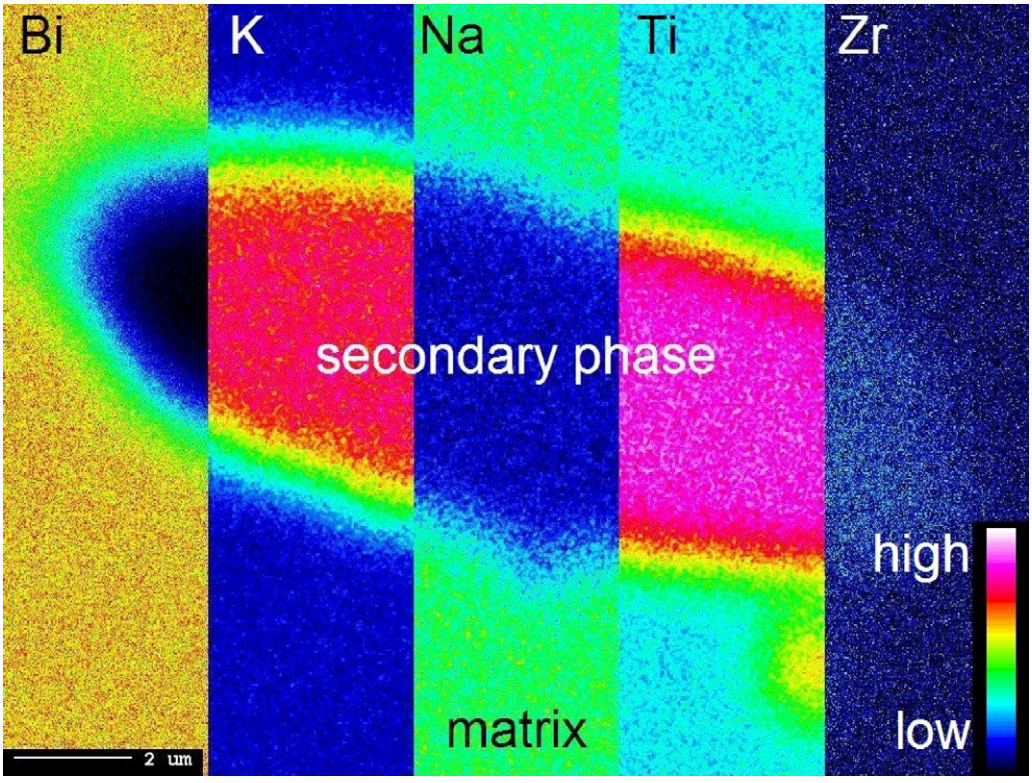

Fig. 5. Elemental distribution in matrix and secondary phase measured with EMPA using WDS detectors. Apparent zoning is caused by the interaction of the electron beam with the material.

Table 2
Composition of matrix and secondary phase determined by EMPA (standard deviation 0.84%, calculated from 43 measurements). Data is normalized to Ti = 1 for perovskite and (Ti + Zr) = 6 for secondary phase. The values in the table show the stoichiometric coefficients.

Sintering temperature	Matrix				Secondary phase				
	Bi	Na	K	Ti	Bi	Na	K	Ti	Zr
Target	0.5	0.375	0.125	1		sum = 2		sum = 6	
1000 °C	0.505	0.410	0.117	1	1.028	0.664	1.416	5.873	0.127
1050 °C	0.509	0.406	0.113	1	0.370	0.348	1.562	5.819	0.181
1100 °C	0.502	0.410	0.112	1	0.046	0.254	1.699	5.897	0.103
1150 °C	0.508	0.414	0.087	1	0.027	0.427	1.574	5.889	0.111

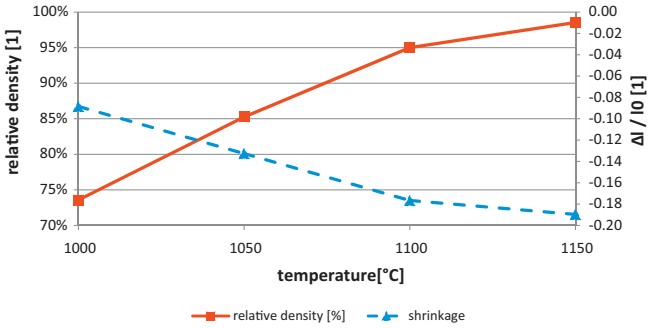

Fig. 6. Density and shrinkage of BNT–25BKT over sintering temperature (sintering duration 5 h).

is Bi_2O_3 evaporating from the secondary phase. The reaction during calcination inflicts the defect and vacancy situation in the material, leading to decomposition during sintering. Both formation reactions of the secondary phase lead to the same compound $M_2Ti_6O_{13}$. The main difference is that the decomposition reaction does not affect the A/B-ratio, nor does it lead to vacancies.

We suggest that the decomposition of the material and the growth of the secondary phase follow Eq. (4). Since BNT and BKT show the same decomposition behaviour[9,10] and Na as well as K form the same compounds with Ti and Zr,[14,15] both are referred to as M:

$$16Bi_{0.5}M_{0.5}TiO_3 \rightarrow M_2Ti_6O_{13} + 10Bi_{0.5}M_{0.5}TiO_3 + \frac{3}{2}Bi_2O_3 + \frac{1}{2}M_2O \quad (4)$$

The most important conclusion from Eq. (4) is that the decomposition does not change the A/B-ratio of the matrix. The formation of the secondary phase creates $M_2Ti_6O_{13}$ and, due to the high sintering temperatures, releases volatile oxides.

Density increases with higher sintering temperatures as expected (Fig. 6).

The low relative density of samples sintered below 1100 °C renders electrical measurements meaningless. The dielectric values for the samples at higher temperatures are presented in Table 3. The polarization curve is also heavily pinched, compared to the ferroelectric loops published (Fig. 7).

Table 3
Dielectric parameters measured at room temperature; $f = 1$ kHz, $V_{rms} = 1$ V.

	ε_r [1]	tan δ [1]	E_C [kV/mm]	P_r [μC/cm²]
BNT–25BKT 1100 °C	1144	0.0726	1.52	16.8
BNT–25BKT 1150 °C	1332	0.0716	0.79	15.8

The characteristic values of the hysteresis loop differs from published data of the BNT–BKT system.[16] Solid solutions of BNT and BKT usually are reported as ferroelectric with standard shaped open hysteresis loops at room temperature. Pinched loops like such presented in this work, are measured at elevated temperatures.[17] Due to different measurement parameters, the values for dielectric properties in the literature are hardly comparable.

4. Summary

It is shown that the critical step in manufacturing BNT–xBKT is the calcination. The formation of BNT–xBKT and $M_2Ti_6O_{13}$ are competing reactions, especially regarding K. The formation of the secondary phase during the calcination reaction leads to a perovskite with a high defect concentration, according to Eq. (2). Those defects destabilize the system at the high sintering temperatures and lead to further formation of the secondary phase. The formation of a secondary phase in sodium deficient BNT has been reported before,[9] this work proposes a mechanism of the generation and growth of these inclusions. Both works indicate that the loss of monovalent ions leads to the decomposition of the ceramic.

According to TGA data (Fig. 2), the material is prone to further decomposition above 1100 °C. The decomposition reaction (Eq. (4)) forms a similar compound, but does not change

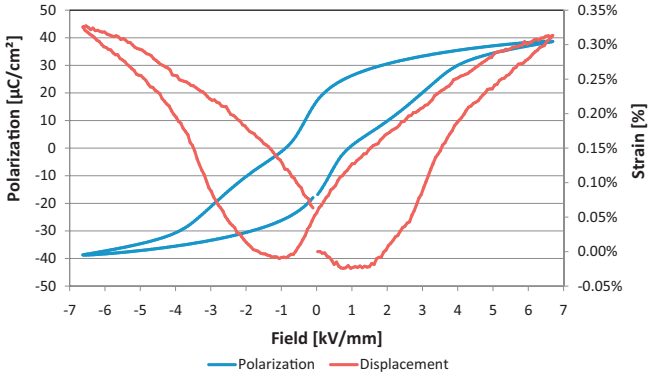

Fig. 7. Hysteresis loop of BNT–25BKT showing pronounced pinching and very low values for E_C and P_R. The saturated polarization is comparable to published values.[16,17] The hysteresis loop was measured with 0.1 Hz at room temperature.

the A/B-ratio of the ceramic since BNT–xBKT decomposes to BNT–xBKT, $M_2Ti_6O_{13}$, Bi_2O_3 and M_2O. Still, the formation of the secondary phase prefers K as the alkali ion, so the decomposition leads to BNT-rich systems. This is the reason for a change of the stoichiometric factor x in BNT–xBKT before and after sintering. The piezoelectric parameters highly differ from published data of comparable compositions. The behaviour of $M_2Ti_6O_{13}$ in electric field is unknown, but its formation influences the stoichiometry and the defect situation in the ceramic.

Acknowledgments

This work was supported by EPCOS OHG, a group company of the TDK-EPC Corporation. Funding was provided by the Christian Doppler Research Association, Austria.

References

1. Haertling GH. Ferroelectric ceramics: history and technology. *Journal of the American Ceramic Society* 1999;**82**(4):797–818.
2. Rödel J, Jo W, Seifert KTP, Anton E, Granzow T, Damjanovic D, et al. Perspective on the development of lead-free piezoceramics. *Journal of the American Ceramic Society* 2009;**92**(6):1153–77.
3. Takenaka T, Nagata H, Hiruma Y. Current developments and prospective of lead-free piezoelectric ceramics. *Japanese Journal of Applied Physics* 2008;**47**(5):3787–801.
4. Aksel E, Forrester JS, Jones JL, Thomas PA, Page K, Suchomel MR, et al. Monoclinic crystal structure of polycrystalline $Na_{0.5}Bi_{0.5}TiO_3$. *Applied Physics Letters* 2011;**98**(15):152901.
5. Hiruma Y, Yoshii K, Nagata HT, Takenaka T. Phase transition temperature and electrical properties of $Bi_{0.5}Na_{0.5}TiO_3$–$Bi_{0.5}A_{0.5}TiO_3$ (A = Li and K) lead-free ferroelectric ceramics. *Journal of Applied Physics* 2008;**103**(8):084121.
6. Isupov VA. Ferroelectric $Na_{0.5}Bi_{0.5}TiO_3$ and $K_{0.5}Bi_{0.5}TiO_3$ perovskites and their solid solutions. *Ferroelectrics* 2005;**315**:123–47.
7. Schmitt LA, Kling J, Hinterstein M, Hoelzel M, Jo W, Kleebe HJ, et al. Structural investigations on lead-free $Bi_{0.5}Na_{0.5}TiO_3$-based piezoceramics. *Journal of Materials Science* 2011;**46**(12):4368–76.
8. Chen P-Y, Chou C-C, Tseng T-Y, Chen H. Second phase and defect formation in $Bi_{0.5}Na_{0.5-x}K_xTiO_3$ ceramics. *Japanese Journal of Applied Physics* 2010;**49**:061506.
9. Spreitzer M, Valant M, Suvorov D. Sodium deficiency in $Na_{0.5}Bi_{0.5}TiO_3$. *Journal of Materials Chemistry* 2007;**17**(2):185–92.
10. König J, Spreitzer M, Jancar B, Suvorov D, Samrdzija Z, Popovic A, et al. The thermal decomposition of $K_{0.5}Bi_{0.5}TiO_3$ ceramics. *Journal of the European Ceramic Society* 2009;**29**:1695–701.
11. Schuetz D, Krauss W, Albering J, Kurta C, Reichmann K. The chemical interaction of silver–palladium alloy electrodes with bismuth-based piezomaterials. *Journal of the American Ceramic Society* 2010;**93**(4): 1142–7.
12. Holleman AF, Wiberg E. *Inorganic Chemistry*. 101st ed. New York: De Gruyter; 1995.
13. Hornbogen E, Skrotzki B. *Mikro- und Nanoskopie der Werkstoffe*; 2009.
14. Dash S, Sood DD, Prasad R. Phase diagram and thermodynamic calculations of alkali and alkaline earth metal zirconates. *Journal of Nuclear Materials* 1996;**228**(1):83–116.
15. Eriksson G, Pelton AD. Critical evaluation and optimization of the thermodynamic properties and phase diagrams of the MnO–TiO_2, MgO–TiO_2, FeO–TiO_2, Ti_2O_3–TiO_2, Na_2O–TiO_2, and K_2O–TiO_2 systems. *Metallurgical and Materials Transactions B* 1993;**24B**(5):795–805.
16. Otoničar M, Škapin SD, Spreitzer M, Suvorov D. Compositional range and electrical properties of the morphotropic phase boundary in the $Na_{0.5}Bi_{0.5}TiO_3$–$K_{0.5}Bi_{0.5}TiO_3$ system. *Journal of the European Ceramic Society* 2010;**30**(4):971–9.
17. Takenaka T, Nagata H, Hiruma Y. Phase transition temperatures and piezoelectric properties of $(Bi_{0.5}Na_{0.5})TiO_3$- and $(Bi_{0.5}K_{0.5})TiO_3$-based bismuth perovskite lead-free ferroelectric ceramics. *IEEE Transaction on Ultrasonics, Ferroelectrics, and Frequency Control* 2009;**56**(8): 1595–612.